Supporting Information

Single-atom catalyst-integrated with semiconductors for constructing a dual-potential electrochemiluminescence sensor for intracellular H_2O_2 detection

Yiran Ying,[#,a] Tianyou Chen,[#,a] Arzugul Ablimit,[b] Chan Zhang,[b] Bing Sun[a], Jing Wu[*,a] and Wu Liu[*,c]

[a]School of Science, China University of Geosciences (Beijing), Beijing 100083, China

[b]Beijing Engineering and Technology Research Center of Food Additives and Beijing Advanced Innovation Center for Food Nutrition and Human Health, Beijing Technology and Business University, Beijing 100048, China

[c]School of Pharmaceutical Sciences, Cheeloo College of Medicine, Shandong University, Jinan 250012, China

*Corresponding authors: Jing Wu (Email: wujing@cugb.edu.cn), Wu Liu (Email: wuliu@sdu.edu.cn)

Table of Contents

1. Experimental Procedures

1.1 Reagents and chemicals

Melamine (99%), cobalt chloride hexahydrate ($CoCl_2 \cdot 6H_2O$, 99.99%), phosphate buffered saline (PBS), molybdenum sulfide (MoS_2, 99%), thiourea (NH_2CSNH_2, 99%), Nafion-117 (5wt.%), glutathione (GSH, 99%), L (+)-cysteine (Cys, 99%), dopamine hydrochloride (DA, 99%) and methyl alcohol (HPLC, ≥99.9%) were purchased from innochem Co. Ltd (Beijing, China). Iron chloride hexahydrate ($FeCl_3 \cdot 6H_2O$, 98%) was purchased from Alfa Aesar (China) Chemical Co., Ltd (Beijing, China). Luminol, glucose (Glu, 99%), *L*-ascorbic acid (AA), uric acid (UA, 99%) and *p*-benzoquinone (BQ) were purchased from Aladdin biochemical technology (Shanghai, China). 5,5-dimethyl-1-pyrroline N-oxide (DMPO) was obtained from Tokyo Chemical Industry Co., Ltd (Shanghai, China). Hydrogen peroxide (H_2O_2, 30% aqueous solution), trypsin-EDTA, acetone and ethanol were brought from Sinopharm Chemical Reagent Co., Ltd (Beijing, China).

1.2 Apparatus

Scanning electron microscopy (SEM) was performed on a JSM-7900 scanning electron microscope (JEOL, Tokyo, Japan) with an accelerating voltage of 3 kV. High resolution transmission electron microscopy (HRTEM) was performed on a JEOL-1400 scanning electron microscope (JEOL, Tokyo, Japan). The aberration-corrected high-angle annular dark-field scanning transmission electron microscopy (AC-HAADF-STEM) was performed by a Titan G2 600 (FEI, United States). X-ray photoelectron spectra (XPS) were recorded on an X-ray photoelectron spectrometer with Al-Kα X-ray (hv = 1486.6 eV) radiation (ThermoFisherEscaLab Xi+, MA, USA). X-ray diffractometer (D8 advance, Bruker, Germany) with Cu Kα radiation (λ = 1.5418 Å) was used to investigate the crystal structures of the samples by collecting X-ray powder diffraction (XRD) spectra with a scan rate of 0.05^o (2θ) s^{-1} in the 2θ range of 5-80°. Electronic paramagnetic resonance (EPR) spectra of $\bullet O_2^-$ and •OH radicals were measured by a Bruker E500 spectrometer under light irradiation. The X-ray absorption fine structure spectra (Co K-edge) were collected at BL14W1 station in Shanghai Synchrotron

Radiation Facility (SSRF). Attenuated-total-reflection Fourier transform infrared spectroscopy (ATR-FTIR) analysis was performed using a Nicolet iS50 FTIR spectrometer (Thermo). Cyclic voltammetry (CV) was measured on a CHI 760e electrochemical workstation (Chenghua Co., Ltd., Shanghai, China) by a three-electrode electrochemical cell system which was composed of a modified glass carbon electrode (GCE) (5 mm diameter) as the working electrode, an Ag/Ag^+ electrode as the reference electrode, and a Pt wire (1 mm diameter) as the counter electrode. ECL was performed with a homemade ECL analyzer which contained a CHI 760e electrochemical workstation and an ultraweak chemiluminescence (CL) analyzer (IFFM-E, Xi'an Remex Analytical Instrument Co., Ltd., China). The electrochemical workstation equipped with the above three-electrode system was utilized to apply the designed voltage. CL analyzer was utilized to take ECL curves.

1.3 X-ray absorption fine structure (XAFS) Measurements

Co K-edge XAFS analyses were performed with Si(111) crystal monochromators at the BL14W Beam line at the Shanghai Synchrotron Radiation Facility (SSRF) (Shanghai, China). Before the analysis at the beamline, samples were placed into aluminum sample holders and sealed using Kapton tape film. The XAFS spectra were recorded at room temperature using a 4-channel Silicon Drift Detector (SDD) Bruker 5040. Co K-edge extended X-ray absorption fine structure (EXAFS) spectra were recorded in transmission mode. Negligible changes in the line-shape and peak position of Co K-edge XANES spectra were observed between two scans taken for a specific sample. The XAFS spectra of these standard samples were recorded in transmission mode. The spectra were processed and analyzed by the software codes Athena.

1.4 Density functional theory (DFT) method

All the DFT calculations were conducted based on the Vienna Ab-inito Simulation Package (VASP). The exchange-correlation effects were described by the Perdew-Burke-Ernzerhof (PBE) functional within the generalized gradient approximation (GGA) method. The core-valence interactions were accounted by the projected augmented wave (PAW) method. The energy cutoff for plane wave expansions was set to 400 eV, and the 2×2×1 Monkhorst-Pack grid k-points were selected to sample the

Brillouin zone integration. The structural optimization was completed for energy and force convergence set at 1.0×10^{-4} eV and 0.05 eV $Å^{-1}$, respectively.

The Gibbs free energy change (ΔG) of each step is calculated using the following formula:

$$\Delta G = \Delta E + \Delta ZPE - T\Delta S$$

where ΔE is the electronic energy difference directly obtained from DFT calculations, ΔZPE is the zero point energy difference, T is the room temperature (298.15 K) and ΔS is the entropy change. ZPE could be obtained after frequency calculation [1]:

$$ZPE = \frac{1}{2}\sum hvi$$

And the TS values of adsorbed species are calculated according to the vibrational frequencies [2]:

$$TS = k_B T \left[\sum_k ln\left(\frac{1}{1 - e^{-hv/k_B T}}\right) + \sum_k \frac{hv}{k_B T} \frac{1}{\left(e^{hv/k_B T} - 1\right)} + 1 \right]$$

2. Supplementary Figures

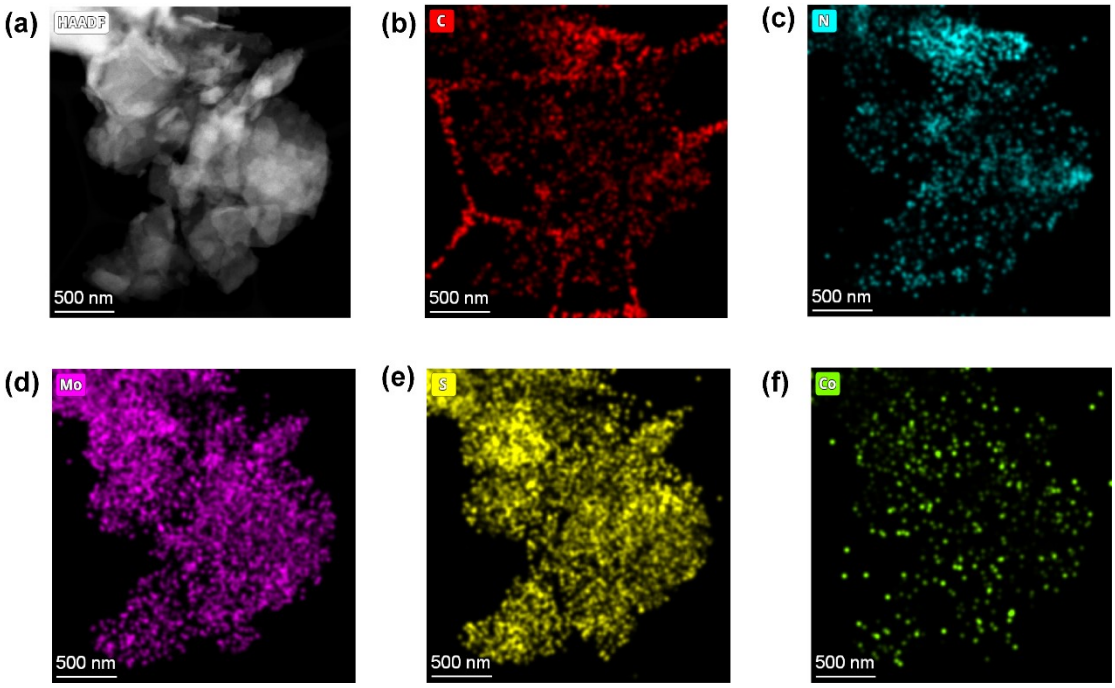

Figure S1. (a) Aberration-corrected high-angle annular dark field scanning transmission electron microscopy (AC-HAADF-STEM) image of MoS_2/Co-C_3N_4 and elemental mapping images: C (b), N (c), Mo (d), S (e), and Co (f).

To analyze the crystalline phase of the prepared catalyst, X-ray diffraction (XRD) measurements were performed. As expected, no new characteristic peaks were observed, except for the 13.0° and 27.4° diffraction peaks attributed to the (100) and (002) crystal faces of g-C_3N_4 (Figure S2a), further confirming that the metal atoms did not agglomerate. The XRD patterns of MoS_2/Co-C_3N_4, MoS_2/Fe-C_3N_4, MoS_2 and g-C_3N_4 were shown (Figure S2b). The characteristic peaks of the (100) and (002) crystal faces of g-C_3N_4 and the characteristic peaks of the (002), (100), (103), and (110) crystal faces of MoS_2 were observed in the composite materials. Additionally, no new peaks were formed, indicating the successful combination of MoS_2 and g-C_3N_4.

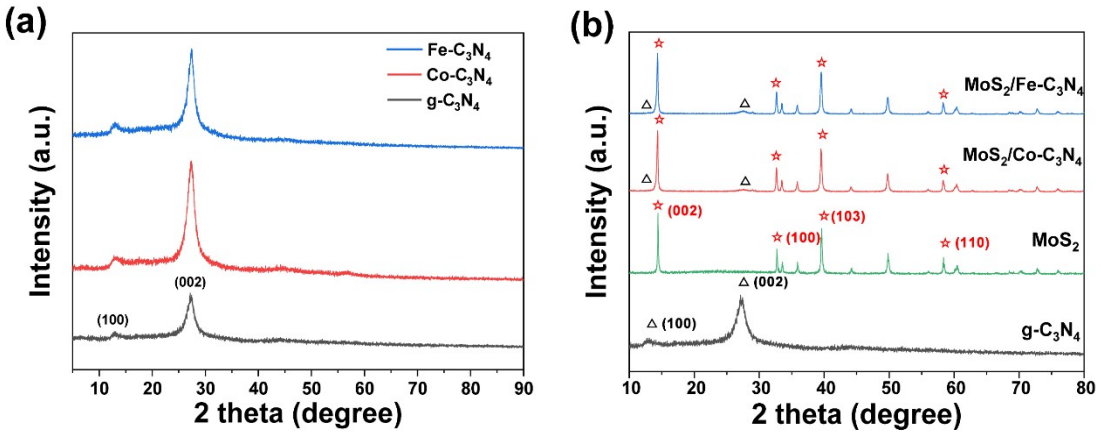

Figure S2. (a) XRD patterns of Co-C_3N_4, Fe-C_3N_4, and g-C_3N_4. (b) XRD patterns of MoS_2/Fe-C_3N_4, MoS_2/Co-C_3N_4, MoS_2, and g-C_3N_4.

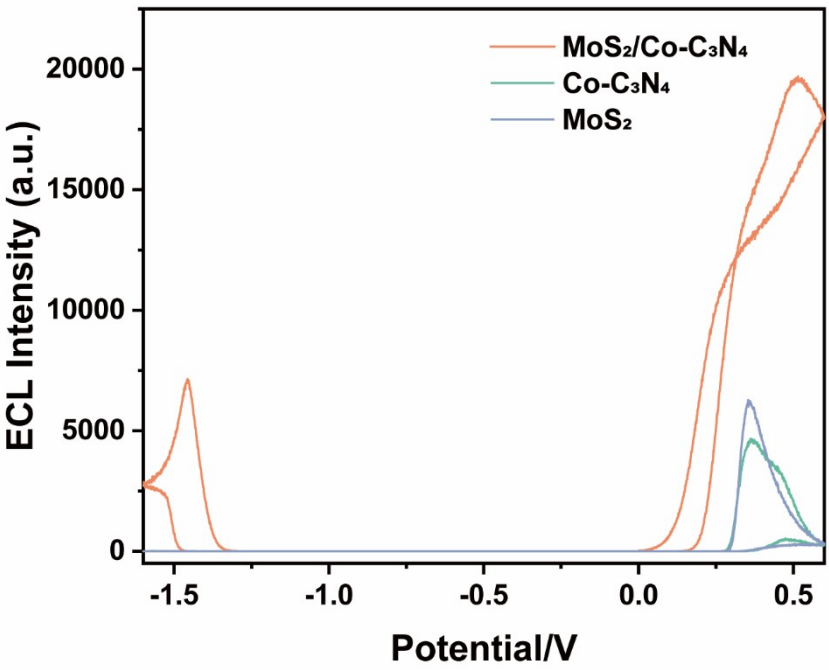

Figure S3. ECL intensity of MoS_2/Co-C_3N_4-modified, MoS_2-modified, and Co-C_3N_4-modified GCE in the luminol-H_2O_2 system (PMT voltage = 900 V, CV parameters: potential range from –1.6 V to 0.6 V, scan rate of 50 mV s^{-1}).

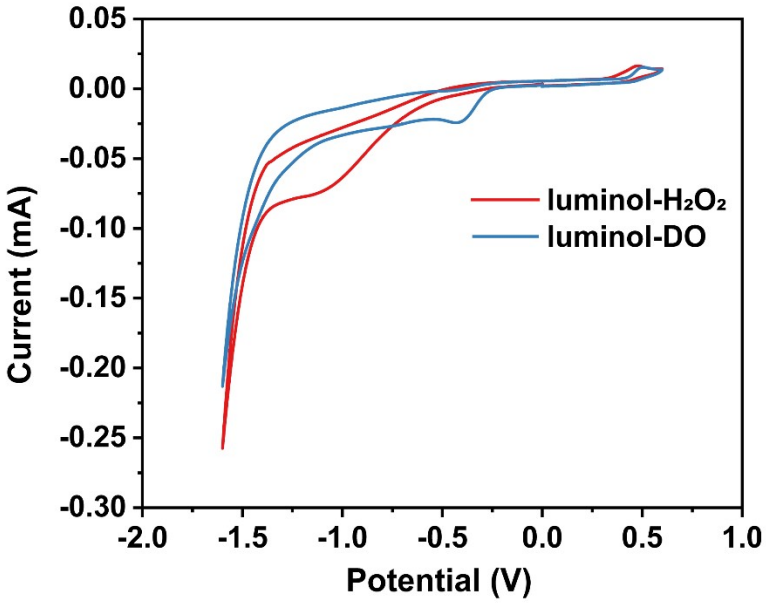

Figure S4. Comparative CV curves of MoS_2/Co-C_3N_4 in the luminol-H_2O_2 system and the luminol-DO system.

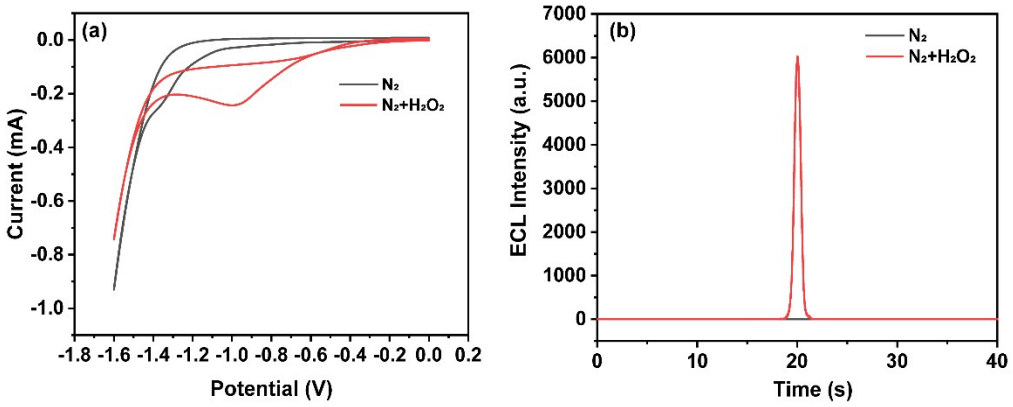

Figure S5. CV curves (a) and ECL intensity (b) of MoS_2/Co-C_3N_4-luminol system in N_2-saturated PBS buffer solution with or without H_2O_2.

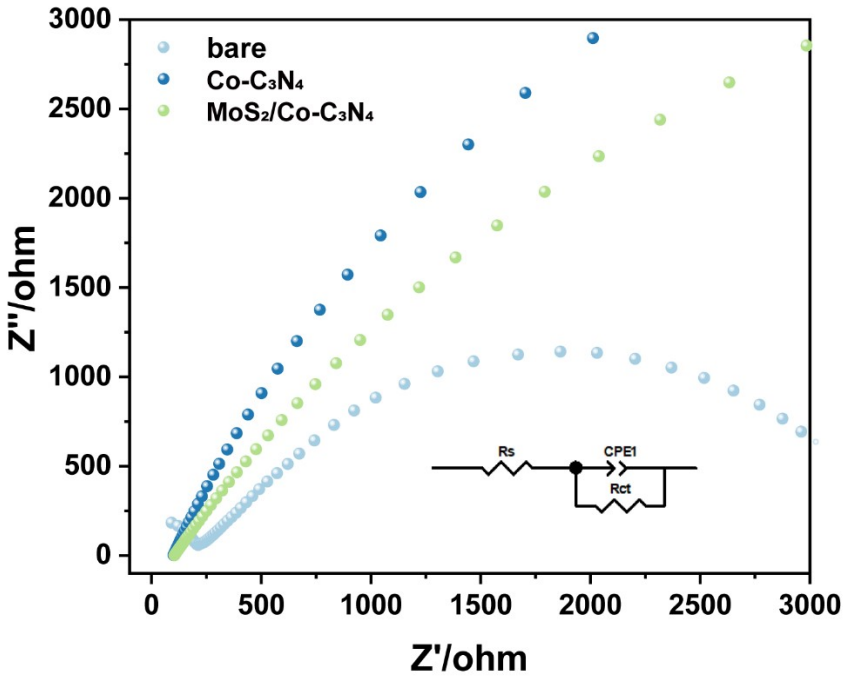

Figure S6. Electrochemical impedance spectra (EIS) of the bare electrode, $Co\text{-}C_3N_4$, and $MoS_2/Co\text{-}C_3N_4$ recorded in 5 mM $Fe[(CN)_6]^{3-/4-}$ solution. Inset: Corresponding equivalent circuit used for fitting. Rs: solution resistance; Rct: charge transfer resistance; CPE: constant phase element.

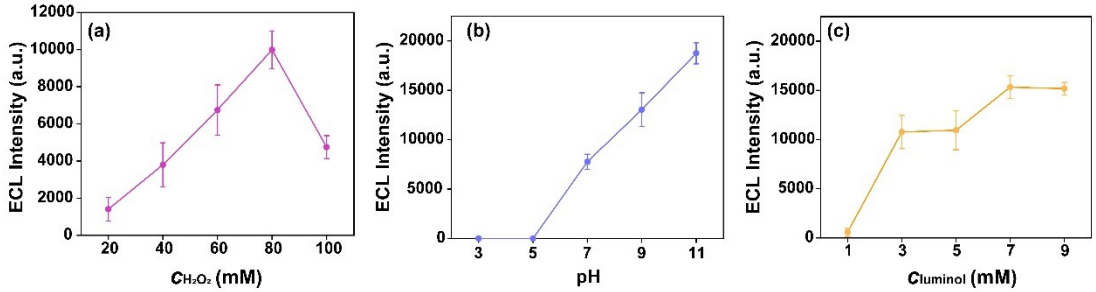

Figure S7. Optimization of reagent concentrations for MoS_2/Co-C_3N_4-luminol-H_2O_2 ECL system: (a) H_2O_2 concentration, (b) pH value, and (c) luminol concentration.

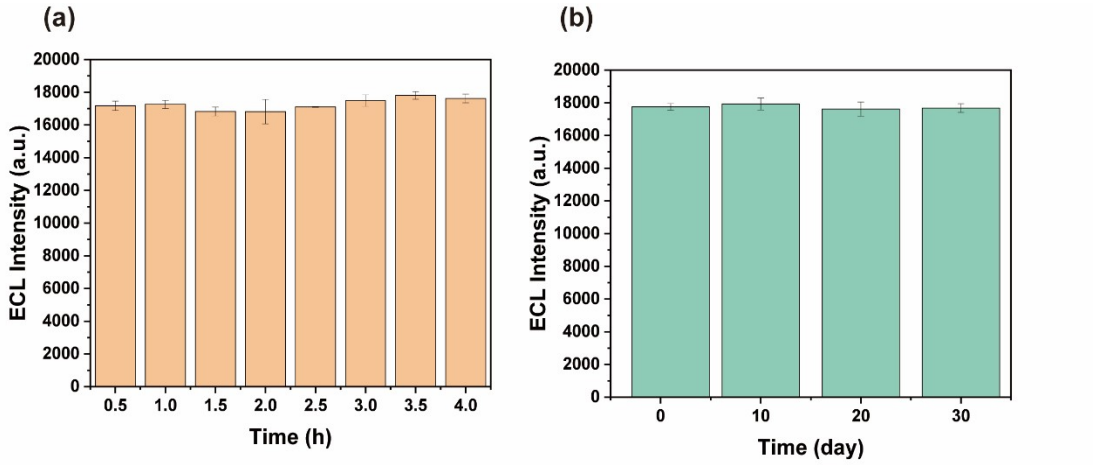

Figure S8. Intraday (a) and interday (b) data of anodic ECL intensity of MoS_2/Co-C_3N_4 under optimal conditions.

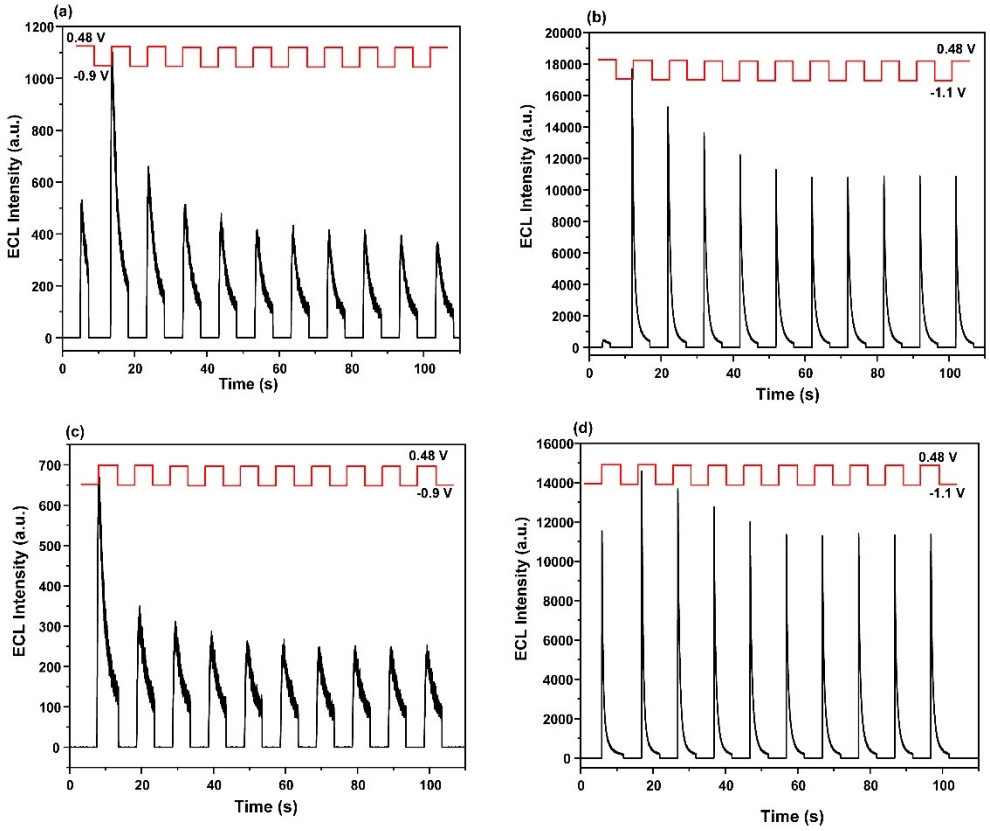

Figure S9. Transient ECL of MoS_2/Co-C_3N_4-luminol-H_2O_2 system under stepwise pulse (SP) conditions within the potential ranges of 0.48 ~ −0.9 V (a), 0.48 ~ −1.1 V (b), −0.9 ~ 0.48 V (c), and −1.1 ~ 0.48 V (d). The red curves represent the applied potential steps.

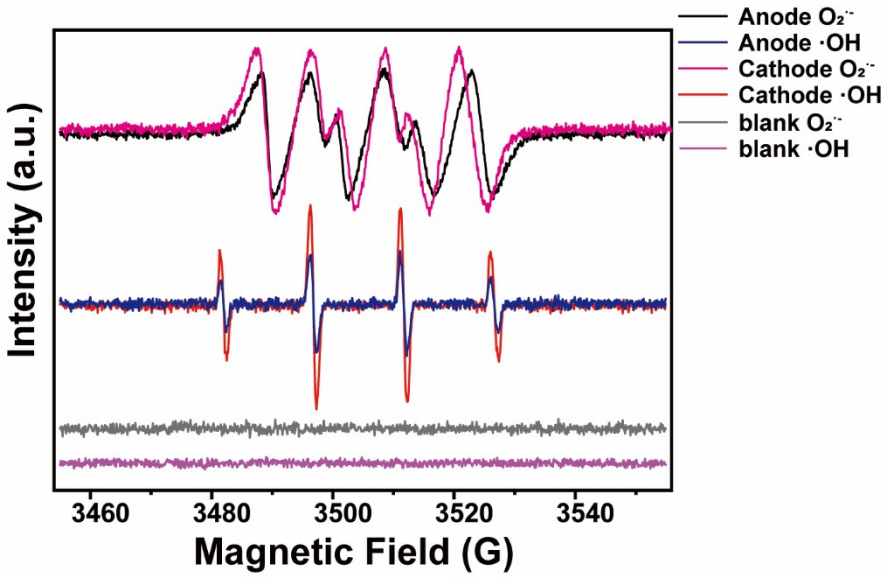

Figure S10. EPR spectra of MoS_2/Co-C_3N_4 and control in H_2O_2.

3. Supplementary Table

Table S1. Local structure parameters around Co estimated by EXAFS analysis of MoS_2/Co-C_3N_4.

Shell	N[a]	***R*** (Å)[b]	σ^2 (Å^2)[c]	ΔE_0 (eV)[d]	R factor
Co-N	2.3 (2)	1.9	0.014	-9.8	0.026
Co-S	0.7 (1)	2.2	0.002		

[a]N = coordination number; [b]*R* = distance between absorber and backscatter atoms; [c]σ^2 = Debye-Waller factor; [d]ΔE_0 = energy shift; R-space fit.

Table S2. Intra-day ECL intensity measurements of MoS_2/Co-C_3N_4.

Time (h)	Measurement 1	Measurement 2	Measurement 3	Mean	Relative Standard Deviation (RSD)
0.5	17038	16988	17512	17179.33	1.61%
1.0	17529	17032	17223	17261.33	1.50%
1.5	16778	16587	17121	16828.67	1.64%
2.0	16216	16581	17652	16816.33	4.39%
2.5	17073	17111	17125	17103.00	0.61%
3.0	17332	17256	17895	17494.33	1.98%
3.5	18021	17850	17556	17809.00	1.34%
4.0	17317	17802	17752	17623.67	1.43%

Paired t-tests were performed between adjacent time points. The critical t-value at df = 2, $\alpha = 0.05$ (two-tailed) is ±4.303. Results are as follows:

Table S3. Paired *t*-test results for intra-day ECL intensity of MoS_2/Co-C_3N_4.

Comparison	Mean Difference (D)	SD of Difference (SD)	t-value	p-value	Significance (α = 0.05)
0.5 h vs 1.0 h	82.00	390.98	0.36	0.748	Not significant
1.0 h vs 1.5 h	-432.66	367.21	-2.04	0.178	Not significant
1.5 h vs 2.0 h	-12.34	738.47	-0.03	0.980	Not significant
2.0 h vs 2.5 h	286.67	738.47	0.67	0.564	Not significant
2.5 h vs 3.0 h	391.33	345.56	1.96	0.186	Not significant
3.0 h vs 3.5 h	314.67	238.25	2.29	0.148	Not significant
3.5 h vs 4.0 h	-185.33	252.19	-2.27	0.150	Not significant

Table S4. Inter-day ECL intensity measurements of MoS_2/Co-C_3N_4.

Day	Replicate 1	Replicate 2	Replicate 3	Mean	Standard Deviation (SD)
1	17886	17514	17850	17750.00	200.92
10	18271	17555	17952	17926.00	366.68
20	17175	17653	18031	17619.67	430.10
30	17371	17811	17852	17678.00	248.07

Paired t-tests were applied to adjacent day-pairs. The results are as follows:

Table S5. Paired *t*-test results for inter-day ECL intensity of MoS_2/Co-C_3N_4.

Comparison	Mean Difference ($\bar{D}$)	SD of Difference (SD)	t-value	p-value	Significance ($\alpha = 0.05$)
Day 1 vs Day 10	176.00	366.68	0.83	0.488	Not significant
Day 10 vs Day 20	-306.33	430.10	-1.23	0.321	Not significant
Day 20 vs Day 30	58.33	248.07	0.41	0.715	Not significant

Table S6. Recovery results and t-test analysis for MoS_2/Co-C_3N_4 toward spiked H_2O_2 concentrations (1, 10, and 100 nM).

Spiked Concentration (nM)	%Recovery (Mean)	%RSD	t-value	p-value	Significance (α = 0.05)
1	94.0%	4.87%	–2.27	0.15	Not significant
10	105.1%	9.85%	0.77	0.51	Not significant
100	97.13%	5.05%	–1.01	0.42	Not significant

The critical t-value at α = 0.05 (two-tailed) is ±4.303.

References

[1] J.K. Nørskov, J. Rossmeisl, A. Logadottir, L. Lindqvist, J.R. Kitchin, T. Bligaard, H. Jónsson, Origin of the overpotential for oxygen reduction at a fuel-cell cathode, J. Phys. Chem. B 108 (2004) 17886-17892

[2] L.I. Bendavid, E.A. Carter, CO_2 adsorption on Cu_2O(111): A DFT+U and DFT-D study, J. Phys. Chem. C 117 (2013) 26048-26059.